University of Groningen

Trigger Efficiencies at LHCb in the Search for $B_s^0 \to e^{\pm}\mu^{\mp}$

Author:
Hilbrand Kuindersma
s1994085

Supervisor:
Dr. Ir. C.J.G. Onderwater

Second examiner:
Prof. Dr. R.G.E. Timmermans

July 12, 2016

Contents

1 Introduction

The Standard Model (SM) is the best description of fundamental particles and forces known today. It is a quantum field theory and every fundamental particle can be seen as an excitation of the corresponding field. For the past 40 years the SM has been a successful theory, describing nature at its fundamental level very well. However, there is a need for extensions of the SM, as its range of applicability is being exceeded.

A striking example of a physics phenomena the SM cannot describe is the mass of the neutrinos. According to the SM, neutrinos should be massless. However, experimental evidence has been found for neutrino oscillations, an immediate sign that neutrinos *do* have mass. Another well known problem is the imbalance of matter and antimatter in our universe. According to the SM, there should be a tiny imbalance. Yet, we observe to live in a matter dominated universe. New physics is needed to give solutions to these problems.

There are several ways physicists have begun to look for new physics, or physics beyond the standard model. At low energy levels, the violation of fundamental symmetries such as CP-violation, is being researched by studying electric dipole moments of fundamental particles. At high energies, forbidden transitions, for example those violating (charged) lepton flavor conservation, are being researched. One of the experiments where the latter happens is LHCb, with its detector located at the Large Hadron Collider (LHC).

The LHC is the particle accelerator run by the European Organization for Nuclear Physics (CERN). Protons are accelerated in both directions of the 27 km long tube until they have a center of mass energy of almost 7 TeV, giving them a speed almost equal to the speed of light. Because of the enormous amount of energy, collisions produce a shower of hundreds of new particles, referred to as "events".

The LHCb detector is one of four main detectors located along the LHC tube. Every detector has its own unique detection capabilities. The LHCb is designed in such a way that it is excellent in distinguishing between electrons, muons, charged hadrons and photons, with hit information gathered from several different detectors parts when the particles fly through. The goal of the LHCb experiment is to study the tiny differences in matter particles and its antimatter conjugates. These results could eventually contribute to new physics, describing the imbalance between matter and antimatter in the universe.

There are many reaction types studied at LHCb, among them, rare B decays such as $B_s^0 \to e^{\pm}\mu^{\mp}$. This decay channel is an example of charged-Lepton Flavor Violation (cLFV). According to the SM, decays involving

cLFV are not allowed to occur in nature. Yet, LFV is observed in neutrino oscillations, which is why cLFV is investigated as well. Finding such decays would be a immediate signal that the SM needs extensions.

The analysis of any decay channel starts with the trigger system of the LHCb detector. The function of the trigger system is to interpret events produced by proton collisions and determine, based on a set of requirements called trigger lines, whether or not an event is interesting for further analysis. It consists of three parts: the level 0 trigger (L0) and two high level triggers (HLT1 and HLT2). In the perfect scenario the system stores all interesting events. However, in reality this will not happen and therefore the efficiency of the trigger system has to be determined. Once the trigger efficiency is known, it is used to determine the branching fraction of the decay channel that is looked for.

Next to a straightforward determination of the efficiency by simulation, it can also be determined using the so-called TISTOS method. This method uses real data only, so no Monte Carlo (MC) simulation of data is needed. Once a decay channel is specified, e.g. $B_s^0 \to e^{\pm}\mu^{\mp}$, the stored events are categorized, in Triggered on Signal (TOS) and Triggered Independent of Signal (TIS). TIS events are immediate hints of the detector inefficiency, as these events were triggered by the background of the event, not by the channel that is looked for. If TIS events happen randomly, the trigger efficiency can be calculated with data only.

This leads to the main goal of this thesis, the determination of the trigger efficiencies of the different LHCb trigger levels. To achieve this, first some theory is required and this will be discussed in **Chapter 2**. In **Chapter 3** and **Chapter 4**, a quick overview is given about the LHCb detector, and the trigger system respectively. Then, in **Chapter 5** the main topic of this thesis is discussed. First, the TISTOS method will be explained and the determination of the trigger efficiency will be discussed. Then, the efficiency of the high level trigger 2 will be determined by simulation of data. Finally, in **Chapter 6**, a discussion and conclusion about the results is given.

Note: *Whenever referred to data in this thesis, it always originated from Run I, i.e. 2011 and 2012.*

2 Theory

To get a good sense of what is happening at the LHCb and why, a little explanation is needed about the problem at hand, the need for new physics. The explanation starts with the fundamental particles and interactions, with added information about composite particles, the hadrons, in Ch. 2.1. In Ch. 2.2, the physics behind lepton flavor violating decays will be discussed. In Ch. 2.3, the search for new physics will be discussed, as well as the role of rare B decays in this search.

2.1 Particles and Forces

The Standard Model (SM) is a quantum field theory describing all fundamental particles as well as the fundamental interactions between them [1]. In this theory, nature is described by quantum fields and fundamental particles can be seen as excitations of these fields. The SM describes 12 fundamental particles types, known as flavors. They are described by Fermi-Dirac statistics and have half integer spin, which is why they are referred to as fermions. Every fermion also has an anti-partner, which has the same mass but opposite charge.

The fundamental interactions, called forces, are in fact the exchange of force carriers called bosons. They are described by Bose-Einstein statistics and have integer spin. Three forces are known from observation today, each with its own force carrier. The photons are the mediators for the electromagnetic force, the $W^{\pm}$ and the Z bosons for the weak force and the gluons for the strong force. Gravitation is sometimes referred to as the fourth force, with hypothetical force carrier the graviton. It is, however, not described by the SM.

The fundamental fermions can be divided into two groups based on the strong force. Quarks interact with each other by means of the strong force, whereas the leptons do not. Both quarks and leptons can be divided into three generations with increasing mass. These generations have two particles each, based on the coupling from the weak force. This leads to the coupling of the up and down, charm and strange, and the top and bottom quarks.

$$\begin{pmatrix} \mathrm{u} \\ \mathrm{d} \end{pmatrix}, \begin{pmatrix} \mathrm{c} \\ \mathrm{s} \end{pmatrix}, \begin{pmatrix} \mathrm{t} \\ \mathrm{b} \end{pmatrix}$$

The leptons on the other hand consist of the electron, muon and tauon, all three with a corresponding neutrino.

$$\begin{pmatrix} \mathrm{e} \\ \nu_e \end{pmatrix}, \begin{pmatrix} \mu \\ \nu_\mu \end{pmatrix}, \begin{pmatrix} \tau \\ \nu_\tau \end{pmatrix}$$

The top and bottom rows are distinguished by their electric charge, $+2/3$ and $-1/3$ for the quarks, and -1 and 0 for the leptons.

The strong force acts on an intrinsic quantum number of quarks, named color [2]. When gluons are exchanged, the color of a quark changes. Possible colors are red, green and blue with corresponding anti-colors. The theory of the strong force, Quantum Chromodynamics (QCD) only allows color neutral states. Also, QCD does not distinguish between flavors in the sense that all quarks have the same amount of color. Therefore, isolated quarks cannot exist and will form hadrons. Hadrons consist of two or more quarks, held together by gluons.

The simplest hadrons are the mesons and baryons. A meson is a quark-antiquark pair and all B mesons contain either a b quark, or a b antiquark. The B_s^0 meson, for example, is a b antiquark together with an s quark. Baryons are particles made out of three quarks, e.g the proton (uud) and the neutron (udd).

2.2 Flavor Physics

Within the framework of the SM, quark flavor is allowed to change in so-called charged current interactions, which is the interaction of the weak force, exchanging a W^+ or W^- and changing the quark flavor. Beta decay is a process involving these current interactions (see fig 1).

A b or s quark can also change into a u quark, because of the three generations. The probability of mixing of quark flavor is described by the Cabibbo-Kobayashi-Maskawa (CKM) matrix [3] [4].

Lepton flavor, on the other hand, should be conserved according to the SM. However, Lepton Flavor Violation (LFV) is observed in neutrino oscillations. Neutrino oscillation is the phenomena where the flavor of a neutrino can oscillate into another flavor after propagation, so $\nu_i \to \nu_j$, where

$i, j = e, \mu, \tau$ and $i \neq j$. Evidence for neutrino oscillation is found in experiments such as [5]. Mathematically analogue to the CKM matrix for quarks, the strength of neutrino mixing is described by the Pontecorvo-Maki-Nakagawa-Sakata (PMNS) matrix [6].

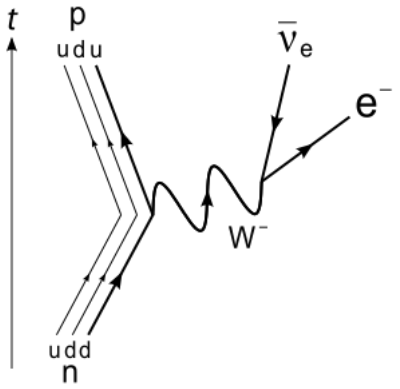

Figure 1: Feynmann diagram of beta decay. A d quark changes into a u quark by exchange of a W^-.

Neutrino oscillation is a clear indication of LFV, physics not described by the SM. Charged LFV, or cLFV, is therefore possible by means of loop diagrams (see fig. 2) for decays such as $\mu \to e\gamma$ and $\mu \to eee$. The branching fractions, i.e. the fraction of decays in a certain mode divided by all possible decay modes, of such cLFV decays within the framework of the SM, taking into account the neutrino oscillations, are of the order of 10^{-50} [7]. This branching fraction is so extremely small, that these types of decays can now, or in the near future, not be observed in nature. If they are observed, it is a immediate signal that the SM needs to be extended with new physics models.

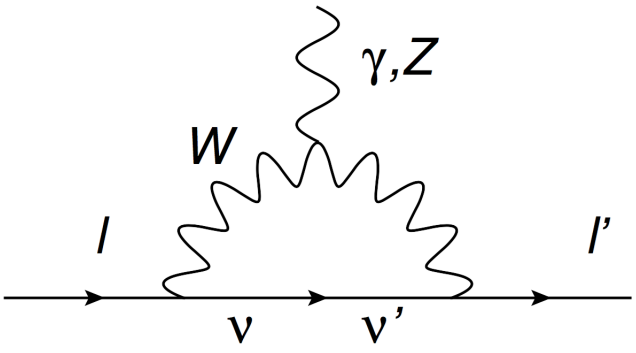

Figure 2: Loop diagram of cLFV by means of neutrino oscillation within the SM [8]

2.3 The Search for New Physics

Since the completion of the current version of the SM in the 1970s, it has been very successful in describing nearly all experimental observations. A few of its predictions were the existance of the W and Z bosons, before they were observed [9]. The latest succes was the discovery of the Higgs boson in 2012, which was predicted more than 50 years ago [10]. However, it should be clear that the SM is beginning to show signs of incompleteness.

There are more physical phenomena the SM is unable to explain. Phenomena such as the imbalance between matter and anti-matter in our universe. Also, it is unable to explain gravity or dark matter. It is clear that there is a need for new physics, or physics beyond the SM.

There are two ways to look for new physics. One can look for new physics directly by testing new theoretical models as extensions to the SM. Supersymmetry is among the most popular theoretical extensions of the SM researched today. In this theory, every elementary particle is coupled to a supersymmetric partner. To test this model directly, the supersymmetric particles would have to be observed. The ATLAS and CMS detectors at the LHC are actively looking for these particles, but have not yet succeeded in finding them [11].

The other way to look for new physics is the indirect approach, by testing predictions made by the SM and find signals where the predictions do not fit observations. That is exactly why physicists around the world are actively looking for rare and very rare decays, among which involve cLFV.

2.3.1 Rare Decays

Rare decays are very well suited to search for new physics, especially when such a decay is forbidden in the SM. New physics models may alter the decay rate significantly, up to the point where they become measurable.

That is why next to leptonic decays at loop level such as $\mu \to e\gamma$, rare B decays are also actively searched for as a probe for new physics, as lepton flavor is also violated. $B_s^0 \to e^{\pm}\mu^{\mp}$ is an example of a semileptonic decay, as leptons are only present in the final state.

The decay channel $B_s^0 \to \mu^+\mu^-$ is also actively searched for. It is not an example of cLFV. However, because its branching fraction is so well described by the SM, it is very sensitive to new physics models [12]. Recent combined observations of CMS and LHCb led to finding the branching fraction of $B_s^0 \to \mu^+\mu^-$ to be $(2.8^{+0.7}_{-0.6})\cdot 10^{-9}$ [13], which is in agreement with the SM prediction. So in this decay mode, no sign of new physics was observed yet. The best upper limit for $B_s^0 \to e^{\pm}\mu^{\mp}$ was found to be $< 1.1(1.4) \cdot 10^{-8}$ at 90% (95%) confidence level [14]. The current analysis aims to improve this.

Another reason to search for new physics models is to explain certain anomalies, observed in rare B-meson decays [15]. New physics models also limit branching fractions of the forbidden decay $D^0 \to e^{\pm}\mu^{\mp}$ to the order of 10^{-8} [16], close to the current upper limit, $< 2.6 \cdot 10^{-7}$ at 90% confidence level, set by the Belle experiment [17].

The LHCb experiment is actively looking for rare B-decays to set an upper limit on branching fractions or to ultimately observing them. How the detector searches for these decays is explained in the next chapter.

3 The LHCb Experiment

The LHCb experiment is one of four main experiments performed at the LHC at CERN. The LHCb detector is designed to be able to distinguish between different types of particles, making it an excellent detector to be used for the search for rare B decays. This chapter will give a brief overview, see ref [18] for a detailed description of the LHCb detector.

First the physics behind proton collisions will be discussed in Ch. 3.1. In Ch. 3.2, the LHCb will be discussed with its main features: the tracking mechanism and particle identification. These features are used in the trigger system, which will be discussed in Chapter 4.

3.1 Proton Collisions in the LHC

The Large Hadron Collider (LHC), based in Switzerland and France, is the largest and most powerful particle accelerator on earth. It is run by the European Organization for Nuclear Physics (CERN) in Geneva, Switzerland.

The accelerator consists of superconducting magnets, used to enhance the energy of particles traversing the tube, increasing their speed with each passage. There are two proton beams traversing is opposite directions that are brought into collision at four different points on the 27 km long LHC tube.

A single proton beam contains 3564 slots and a single slot can contain up to 10^{11} protons [19]. At the collision points , the beams cross each other every 25 ns, resulting in a maximum crossing rate of 40 MHz. However, not all slots are filled with protons. In 2011 and 2012, only 1380 slots were filled and the effective crossing rate is

$$\nu_{eff} = \frac{1380}{3564} \cdot 40 \text{ MHz} \approx 15 \text{ MHz}. \tag{1}$$

The luminosity of the LHC is a very important parameter. It contains information about compactness of the beams, the number of protons per slot and the crossing rate of these slots. The luminosity at the interaction point of the LHCb, where the protons are brought into collision, was $L = 4 \cdot 10^{32}$ cm^{-2} s^{-1} for Run I.

The amount of inelastic proton collision in a period Δt that occur when filled slots cross each other can be calculated by the proton-proton cross

section $\sigma_{pp,inel}$ multiplied by the integration of the luminosity L over time:

$$N_{tot} = \sigma_{pp} \int_0^t L \, \mathrm{d}t. \tag{2}$$

$\sigma_{pp,inel}$ was calculated to be around 75 mbarn for an center of mass energy of $\sqrt{s} = 7$ TeV, valid for run I [20].

Now, the amount of events[1] per slot crossing[2] can be calculated to be

$$N = \frac{L \cdot \sigma_{pp,inel}}{\nu_{eff}} = \frac{4 \cdot 10^{-32} \text{ cm}^{-2} \text{ s}^{-1} \cdot 75 \cdot 10^{-27} \text{ cm}^2}{15 \cdot 10^9 \text{ s}^{-1}} = 2. \tag{3}$$

These events can possible be detected and how they can be identified will be discussed in the next section.

3.2 The LHCb Detector

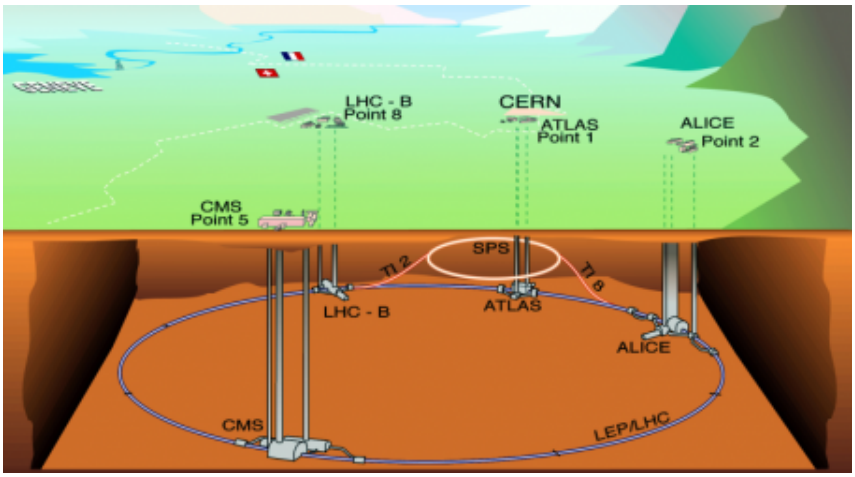

Figure 3: Schematic overview of the LHC and the location of the four detectors

.

[1]From now on, inelastic collisions which produce large amount of particles that fly through the detector will be referred to as events.

[2]In reality, the number of collisions per slot crossing is Poisson distributed with a mean of 2.

This section relies strongly on references [19] and [18] unless stated otherwise. The detector of LHCb is located at one of the four point where the proton beams are brought together to collide. The other detectors belong to the ALICE, ATLAS and CMS experiments (see fig. 3).

The detector of LHCb is a spectrometer, covering one way of the beam collision direction (see fig. 4). The pseudorapidity for the LHCb detector lies between $2 < \eta < 5$, where

$$\eta = -ln(tan(\frac{\theta}{2})), \tag{4}$$

with θ being the angle of a scattered or produced particle with respect to the beam axis.

Two important features of the LHCb detector are the tracking system and the Particle Identification (PID) system. The tracking system is used to reconstruct the tracks of the particles that fly through different parts of the detector. The sub-detectors of the LHCb that together make the tracking system are discussed briefly in section 3.2.1. The elements of the PID system, discussed in section 3.2.2, make it possible to distinguish between charged hadrons, electrons, photons and muons.

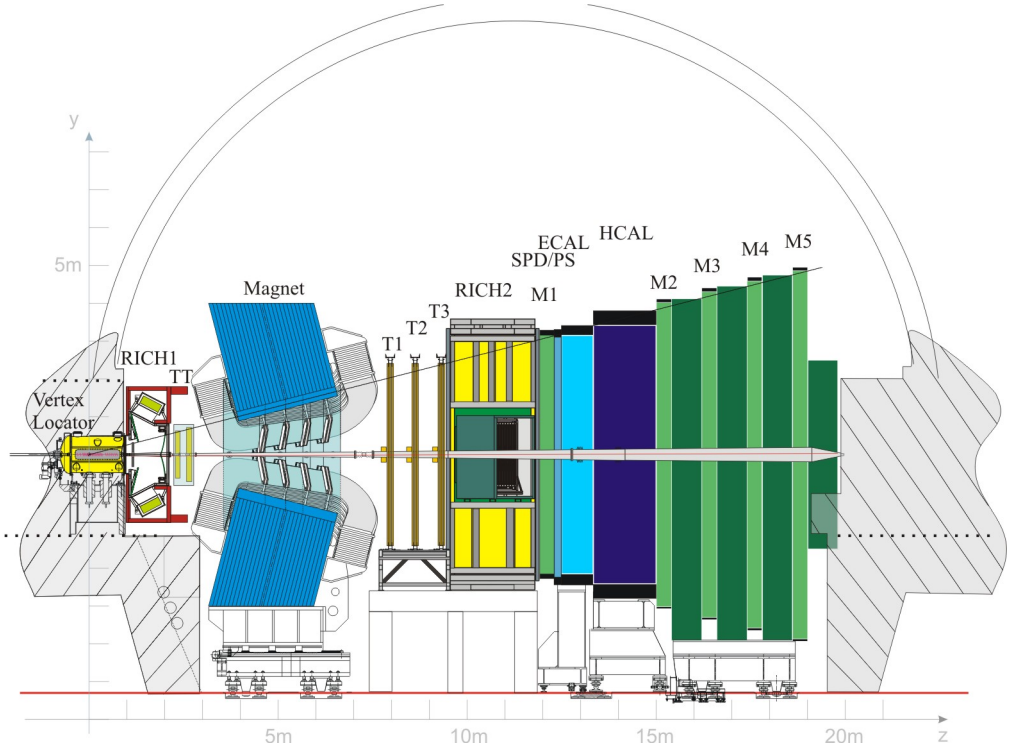

Figure 4: Different sub-detectors within the LHCb detector. The proton beam runs from left to right and vice versa in the middle of the detector. The proton beams are brought together to collide within the Vertex Locator

3.2.1 Tracking

The tracking system consists of:

- Vertex Locator (VELO)
- Tracker Turicensis (TT)
- Dipole magnet
- Three tracking stations (T1-T3)

The VELO is, just like the TT and the innermost part of T1-T3 (IT), a silicon micro strip detector. It is located at the far left side of the LHCb detector in figure 4, around the point where the proton beams are brought into collision. It is used to identify the primary vertex (PV), i.e., the point where two protons collide. In the collision, quarks are produced, which can hadronize to form mesons and baryons. The point where these decay is referred to as the secondary vertex (SV), which the VELO can also identify. See figure 5 on how such a collision within the VELO looks like.

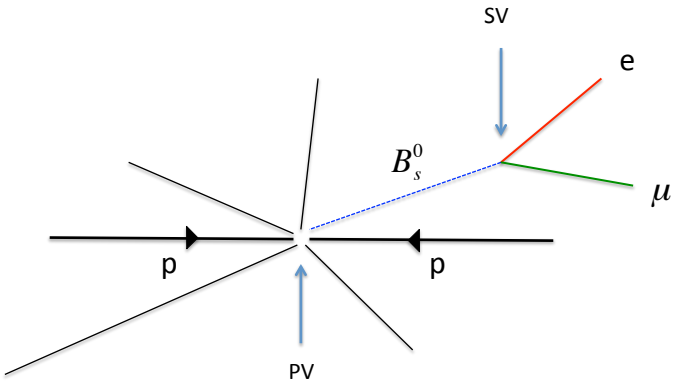

Figure 5: Proton collision producing a B_s^0 meson which decays to an electron and a muon.

The TT is located immediately before the dipole magnet, and the IT after. Both components are used to determine the curvature of a particle through the magnet and from that the momentum p and transverse momentum p_T. The outer part of the T1-T3 is called the Outer Tracker (OT). When a particle travels through the OT, electronics in the system can measure this and the hits are recorded.

Together with the information from the VELO, the OT and IT, the particle's momentum and position are known with relative certainty. With this information, a track can be reconstructed[3], which is used in the trigger system (see Ch 4).

3.2.2 Particle Identification

The PID system consists of:

- Two Ring Imaging Cherenkov detectors (RICH1 and RICH2)
- The calorimeter system (SPD, PS, ECAL, HCAL)
- The Muon detection system (M1-M5)

When particles move through a medium with a speed larger than the speed of light in that medium, they emit photons in the form of a cone

[3]For technical details on how the tracks are reconstructed, see [21]

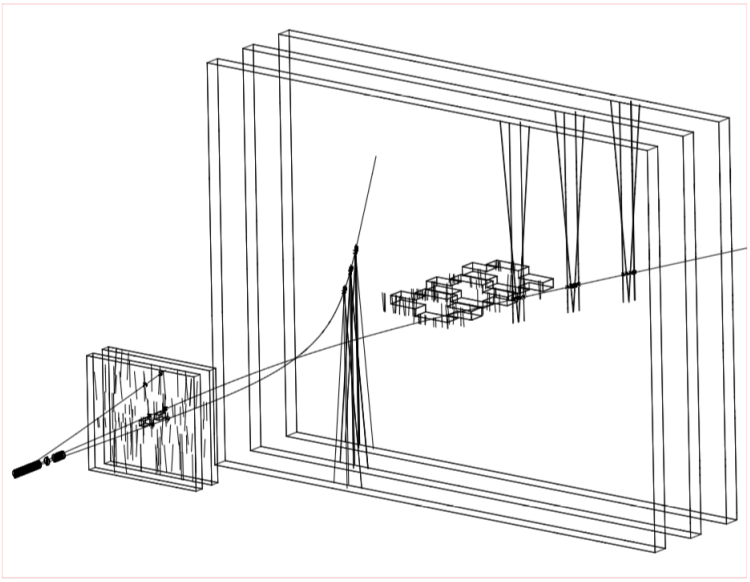

Figure 6: Information from VELO and T1-T3 are used to reconstruct the particle track. [21]

known as Cherenkov radiation. The relation between the angle of the cone and the speed of the particle is given by

$$cos(\theta_c) = \frac{1}{n\beta} \tag{5}$$

Where n is the refractive index of the medium and $\beta = v/c$, c being the speed of light in vacuum.

Kaons, pions and muons move through the detector at different speeds, producing cones with different angles. The RICH1 and RICH2 detect the photons and with this information, θ_c can be determined and the speed β of the particle can be calculated. Then, with β and information about the momentum from the tracking system, the mass of the particle can be reconstructed.

The electromagnetic and hadronic calorimeters, ECAL and HCAL, measure energy losses of the particles. Electrons and photons deposit energy in the ECAL. The HCAL is positioned after the ECAL, and the electrons and photons will therefore usually only leave a small fraction of energy in the HCAL. Hadrons however, usually have more energy, which they deposit in the HCAL more easily.

Muons on the other hand, deposit almost no energy in the calorimeters so a muon detector is needed. It is the last part of the detector which is

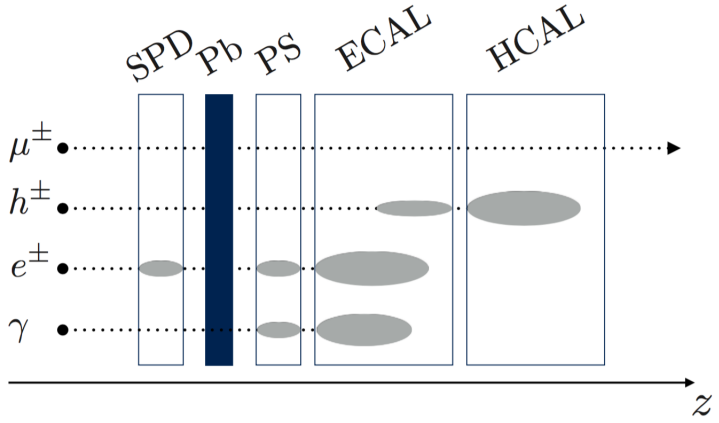

Figure 7: Different particles deposit their energy predominantly in different parts of the calorimeter system [19]

also located at the end of the detector in figure 4. It consists of five muon detectors. M1 is located before the calorimeters and M2-M5 are located behind. M1-M3 are used to calculate the transverse momentum of particles flying through. M4 and M5 are used to identify particles that have been misidentified as muons in M1-M3.

With the complete information from the tracking system, tracks can be reconstructed. With the information from the PID system, particles can be associated with these tracks. The trigger system can now analyze these tracks and based on a set of requirements it can store events or delete them. The complete trigger procedure is discussed in the next chapter.

4 Trigger System of LHCb

Before any analysis of $B_s^0 \to \mu^\pm e^\mp$ at the LHCb can be done, data of events including this decay channel is needed. Because the branching fractions of this channel is $< 10^{-8}$ (section 2.3), an enormous amount of decays of the B_s^0 are needed to observe it. Typically, $1.5 \cdot 10^7$ collisions between protons slots occur every second in LHCb, with every collision typically producing hundreds of particles. This number is too large to be able to store every detail of every single event to disk. Therefore, a trigger system in the LHCb has to reduce this number by deleting uninteresting events.

First, an event has to pass the Level-0 trigger (L0), which is discussed in Ch. 4.1. The events that pass the L0 are then analyzed by the High Level Trigger (HLT) which consists of two parts. The HLT is discussed in Ch 4.2. All events that also pass the HLT are stored permanently, in the form of a trigger report for further analysis. See [22] and [23] for a detailed discussion about the trigger performance in 2011 and 2012 respectively on which this section relies strongly. See [18] for technical details about the trigger system.

4.1 Level-0 Trigger

The rate of visible interactions created by the proton-proton collisions within the LHCb detector (see section 3.1) is about 15 MHz. Particles created in the events fly through the LHCb detector, leaving hits in the tracking and PID systems (see section 3.2). The L0 makes the first selection of which events to delete to reduce this number to around 1 MHz.

The L0 is implemented in the hardware of the detector. The three components of the L0-trigger are the muon, calori and the pilup[4] triggers. The reconstruction of events is used in the HLT1 and HLT2. So the L0 decision is based on hits only and no reconstruction is involved yet.

The muon trigger processes the hits in the muon detectors (M1-M5). It selects events containing at least one muon. It also selects events containing a muon pair with a high chance of originating from the same particle, which is important for other analyses such as $B_s^0 \to \mu\mu$. Because muons can also be created in processes other than $pp \to b\bar{b} \to B_s^0 \to e^\pm\mu^\mp$, i.e. in the background, only muons with transverse momentum $p_T > 1.76$ GeV are selected. Muons with lower p_T, most likely do not originate from an interesting decay. The rate of events containing a muon meeting the criteria is about 0.4 MHz.

The calori trigger uses information from the ECAL and HCAL. Because the different particles that fly through the detector all have different penetrat-

[4]The pile-up trigger is used to determine the luminosity and not relevent for B physics [22] and is therefore not discussed in this thesis

ing power. The calori trigger can distinguish between them. When a large enough amount of energy ($E > 3.68$ GeV) has been deposit in the HCAL, the event is triggered as containing a hadron. This applies also to electromagnetic particles for the ECAL, when at least $E > 3$ GeV is deposited. The rate of events containing a hadron or an electromagnetic particle meeting the criteria is about 0.6 MHz. Together with the muon output this gives a total output of the L0 trigger of about 1 MHz for the HLT to process. See table 1 for the complete selection criteria and output of the L0-trigger.

Table 1. L0 tresholds and output rate [23].

	2011 (GeV)	2012 (GeV)	L0 output rate (MHz)
p_T single muon	1.48	1.76	0.15
p_T double muon	1.96^2 (GeV^2)	1.6^2 (GeV^2)	0.25
total muon			0.4
E_T hadron	3.5	3.7	0.45
E_T electron/photon	2.5	3	0.15
total hadron & EM			0.6

4.2 High Level Trigger

The HLT runs on software on 29,000 computers in the Event Filter Farm (EFF). Based on a series of selection alorithms it is in principle able to reconstruct the complete event. However, about two seconds per event are needed for this process and it has to analyse roughly around a million events per second. Therefore, the HLT is divided into two steps; the HLT1 and HLT2. Each step performs a partial reconstruction. Both steps are discussed below.

The HLT1 is fast enough to be able to reconstruct VELO tracks of all output events of the L0. Events triggered by the L0 muon trigger are picked out by the HLT1 and the VELO tracks are reconstructed. Then, the tracks are extrapolated to the M3 detector. If hits are found within a specified search regime in M3, then M2, M4 and M5 are checked for additional hits. If, next to the hit in M3, another hit is found, the event is marked as including a muon. Other events from the L0, i.e. events that were not triggered by the L0 muon, are marked, based on a quantity called Impact Parameter (IP). This is the distance from the PV determined by the VELO and the reconstructed VELO track. If the IP is small enough, the event is marked.

All marked events, either by IP or muon detection, are further reconstructed. This process is called forward tracking. For details on forward tracking see [24]. This procedure uses information from the IT and OT, to determine the momentum of the particles. Just like in the L0 trigger for the muon trigger, the particles must have p and p_T greater than a specified value to be triggered. These requirements are called trigger lines. The HLT1 has about 38 different trigger lines and if the requirements of at least one is met, the event is triggered. The output rate of the HLT1 was about 80 kHz in 2012.

The HLT2 is now able to perform forward tracking for all VELO tracks. However, only VELO tracks with high enough p and p_T are checked (5 GeV and 0.5 GeV resp.). Because in the HLT2 a complete reconstruction of the tracks is available, more requirements can be made, resulting in about 130 different trigger lines. Just as in HLT1, if the requirements of at least one is met, the event passed HLT2. The final output rate of the HLT2, the number of "triggered" events, was about 5 kHz in 2012. These events are stored permanently in the form of trigger reports (see Ch. 5.1). The output can be divided into two important event groups in the search for B decays [19]:

• Generic beauty lines. Triggered because a b-hadron decay with at least two charged tracks was reconstructed, e.g. $B_s^0 \to \mu^{\pm} e^{\mp}$, but also tracks such as $B_s^0 \to hh$

• Muonic trigger lines. Triggered because there was at least one muon in the final state, e.g. $B^+ \to J/\psi K^+ \to \mu\mu K^+$

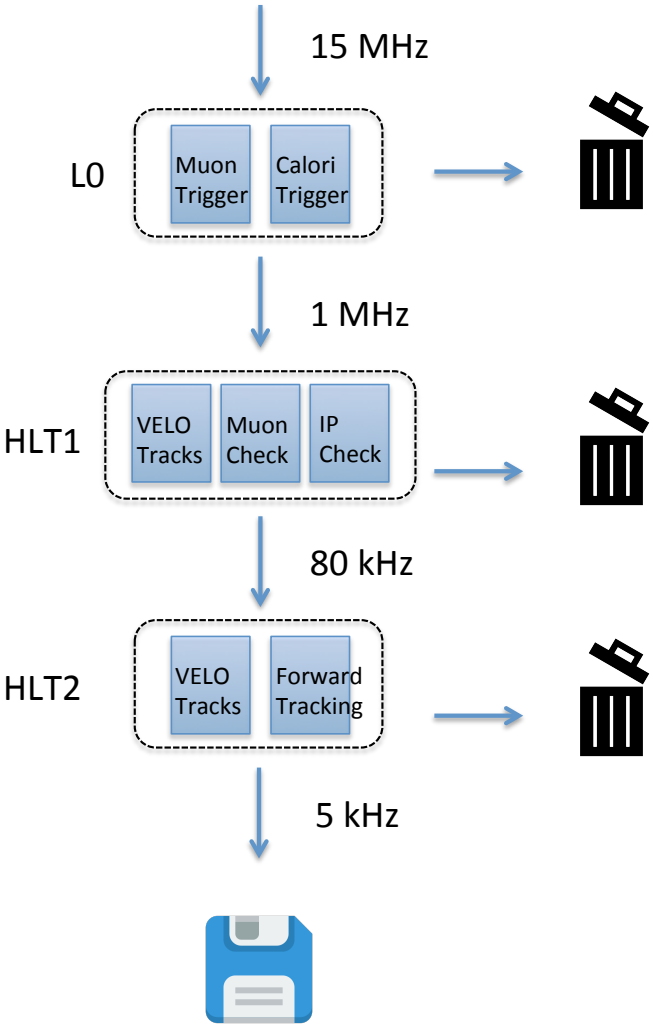

Figure 8: The different levels of the trigger system including input and output event rates (2012).

5 Trigger efficiency

When all data is collected, it can be analyzed. The goal of the analysis is to determine the branching fraction of $B_s^0 \to \mu^{\pm} e^{\mp}$. The branching fraction depends on many aspects, one being the complete efficiency of the experiment ϵ_{tot}. This in turn, depends on several efficiencies throughout the detector, as well as efficiencies in the readout and analysis of the events.

When an events occurs, i.e. two protons collide and produce particles, it does not always occur within the detector detection window. Resulting in a detection efficiency ϵ_{det}. When the event does happen within the detection window, it can be triggered. However, the trigger system can sometimes misidentify events or completely miss an interesting event. This leads to a trigger efficiency on events that have passed the detection $\epsilon_{det \to trig}$. Events that have been triggered are then stored to disk as data. Software is then used to reconstruct the tracks and identify the particles leading to a reconstruction efficiency on events that have been triggered $\epsilon_{trig \to rec}$. Once the events are reconstructed, they are selected as containing the decay channel searched for, given the final efficiency $\epsilon_{rec \to sel}$. This gives a total efficiency of:

$$\epsilon_{tot} = \epsilon_{det} \cdot \epsilon_{det \to trig} \cdot \epsilon_{trig \to rec} \cdot \epsilon_{rec \to sel} \tag{6}$$

So when referring to the trigger efficiency, it actually means the number of events that are triggered and thus have passed the detection, divided by the total amount of events that should have been triggered, which are all the events within the detection window of the detector

$$\epsilon_{det \to trig} = \frac{N_{det \to trig}}{N_{det}} \tag{7}$$

Now, because the trigger system only stores events that are triggered, N_{det} is not known. A straightforward simulation of the trigger system can be used to determine this. However, the L0 trigger is hardware based and the HLT1 trigger uses only a partial reconstruction. It is hard to reproduce these conditions in a simulation. Therefore, an alternative approach has to be made. The TISTOS method can be used to rewrite equation (7) is such a way, that all quantities can be determined from data. The efficiency of the HLT2 *can* be determined with simulation, because the trigger uses the same reconstruction as is made offline. These conditions can be reproduced in a simulation.

To use the TISTOS method, events have to be categorized and how this is done is explained in Ch. 5.1. In Ch 5.2, the determination of the trigger efficiency will be given. In Ch. 5.3, the method to determine the efficiency of HLT2 by means of simulation will be explained and results are given.

5.1 Categorization of TISTOS method

The method starts by specifying the decay to search for: $B_s^0 \to e^{\pm}\mu^{\mp}$, referred to as the signal decay. The data used is stored in the form of a trigger report. This trigger report contains the complete hit information of the events, i.e. information about where exactly the particles flew through different detector parts. Therefore, a complete offline reconstruction can be made.

The trigger report also contains information of the online reconstruction made in the trigger system. The events needed to pass certain requirements known as trigger lines (see Ch. 4). These requirements were tested on the online (partially) reconstructed tracks and based on this the event was stored or not. Because the online reconstruction is not perfect, there are inefficiencies involved.

When the offline reconstruction is made, it can be compared to the online reconstruction and see what was the reason that the event was triggered. An important realization to be made here is that every offline reconstructed event now contains a $B_s^0 \to e^{\pm}\mu^{\mp}$ channel in it, or at least meets the criteria set for it to contain it.

There are four different ways an events can be triggered, leading to the four categories (see fig. 9). These are:

- *Triggered On Signal* (**TOS**): Events triggered because the trigger system recognized the decay channel. Nothing else in the event, i.e. the background, was interesting enough for the trigger to pass the event. If the $B_s^0 \to e^{\pm}\mu^{\mp}$ was not present in this event, it would not have been triggered at all.

- *Triggered Independent of Signal* (**TIS**): Events where the $B_s^0 \to e^{\pm}\mu^{\mp}$ was not recognized. Fortunately, something in the background was interesting enough for the trigger to pass the event. This category is an immediate hint of trigger inefficiency, as the event should have been triggered on the signal decay.

- *Simultaneously TIS and TOS* (**TISTOS**): In these events, the $B_s^0 \to e^{\pm}\mu^{\mp}$ was recognized, but there was also something in the background interesting enough. So even if the signal decay was not detected by the trigger system, the event would have passed either way and vice versa.

• *Triggered On Both* (**TOB**): In these events, information was needed from the decay signal as well as the background. Information from either one was insufficient for the trigger to fire. Because $< 0.05\%$ of all events are TOB, this is not relevant for the analysis.

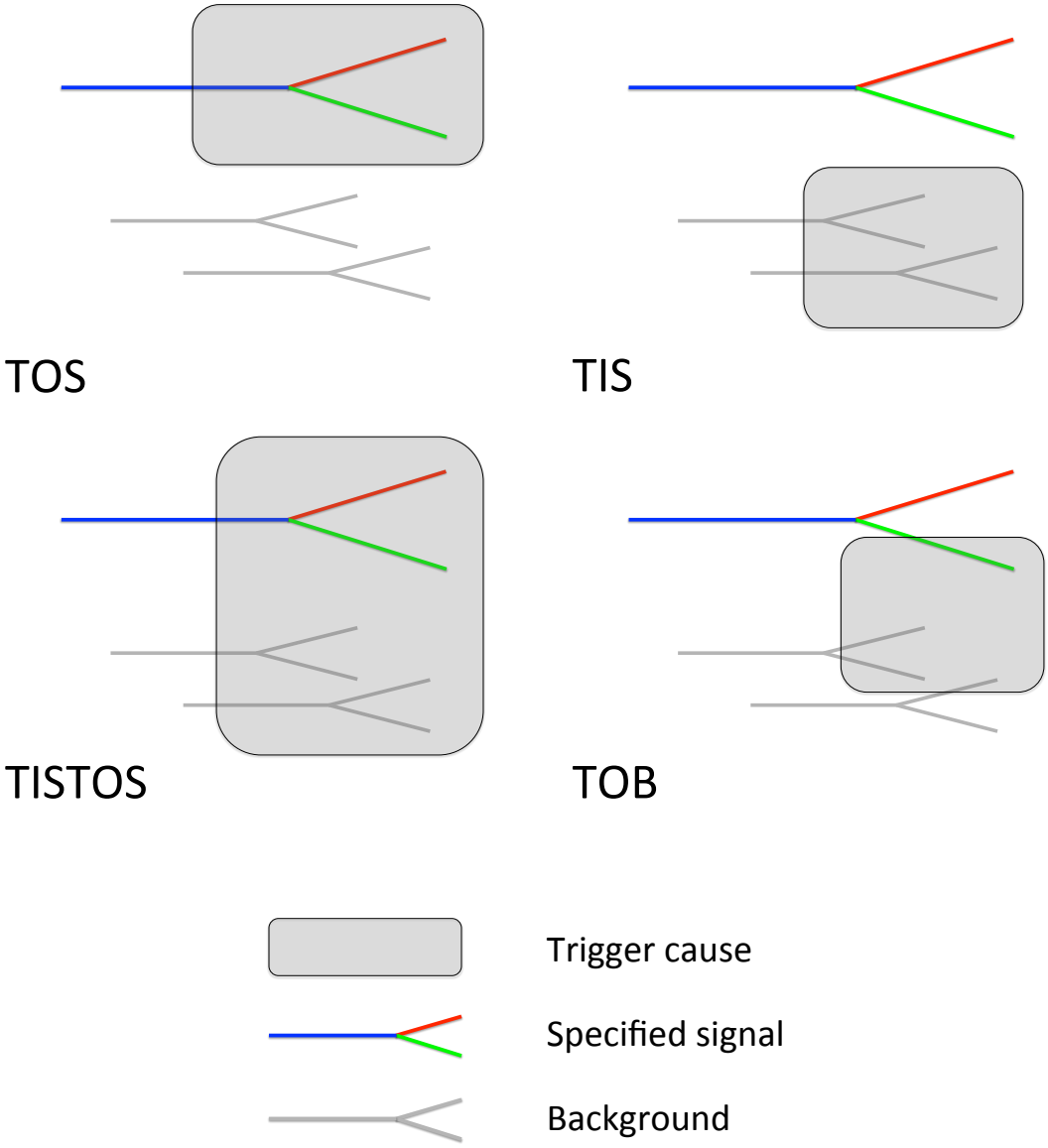

Figure 9: Categorization of the TISTOS method. Note that in the picture the background consists of only two decay channels, while in reality the background can consist of hundreds of different channels.

5.2 Determination of the Efficiency

Now that the events are categorized, the efficiency can be calculated. We know that;

$$\epsilon_{tot} = \epsilon_{det} \cdot \epsilon_{det \to trig} \cdot \epsilon_{trig \to rec} \cdot \epsilon_{rec \to sel} \tag{8}$$

And

$$\epsilon_{det \to trig} = \frac{N_{det \to trig}}{N_{det}}. \tag{9}$$

N_{det} is not known, so another way of determining $\epsilon_{det \to trig}$ is needed.
To be able to apply the TISTOS method, the order of equation (8) has to be rewritten. The TISTOS method determines the trigger efficiency of a specific decay channel of you final selection of events, so we want something of the form:

$$\epsilon_{tot} = \epsilon_{det} \cdot \epsilon_{det \to rec} \cdot \epsilon_{rec \to sel} \cdot \epsilon_{sel \to trig}. \tag{10}$$

This is allowed, because now the trigger efficiency is defined as the number of events in your final selection divided by the number of events that should have been in your selection. The selection and reconstruction efficiencies are still taken into account in the calculation of ϵ_{tot}. We now define

$$\epsilon_{trig} \equiv \epsilon_{sel \to trig} = \frac{N_{sel \to trig}}{N_{sel}} \equiv \frac{N_{trig}}{N_{tot}} \tag{11}$$

for an easier notation.

N_{tot} is at this point still an unknown. We now rewrite equation (12) by multiplying by N_{TIS}/N_{TIS},

$$\epsilon_{trig} = \frac{N_{trig}}{N_{tot}} = \frac{N_{trig}}{N_{TIS}} \cdot \frac{N_{TIS}}{N_{tot}}, \tag{12}$$

Where N_{TIS} are the number of events categorized as TIS. The events in the other two categories are N_{TOS} and N_{TISTOS}. With these, partial efficiencies can be defined as

$$\epsilon_i = \frac{N_i}{N_{tot}}, \tag{13}$$

where i can be either TIS, TOS or TISTOS. Note that $N_{trig} = \sum_i N_i$.

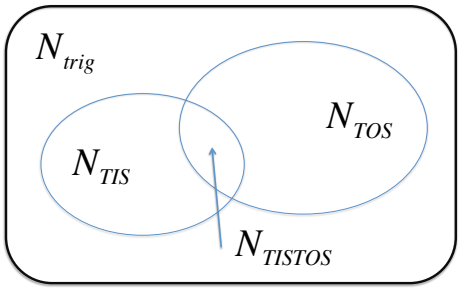

Figure 10: The TIS-events in the TOS subsample are in fact events categorized simultaneously TIS and TOS

Now, the trigger efficiency is

$$\epsilon_{trig} = \frac{N_{trig}}{N_{TIS}} \cdot \frac{N_{TIS}}{N_{tot}} = \frac{N_{trig}}{N_{TIS}} \cdot \epsilon_{TIS}. \tag{14}$$

At this point, it is very important to realize that an event is categorized as TIS, TOS or TISTOS, always with respect to a specified decay channel, the signal decay. If one were to change this signal decay, and started to categorize the events again, some of the events in the channel specified before would fall in other TIS, TOS and TISTOS categories. This is because the decay channel specified first, can be background in the channel specified second, which may or may not have caused a trigger.

N_{trig}, the total number of triggered events and N_{TIS}, the total number of events labeled TIS, are known from the data. ϵ_{TIS} on the other hand is not, so another step has to be made. Because some of the TIS and TOS events overlap, i.e. events can be labeled simultaneously TIS and TOS (TISTOS), we can define the efficiency of TIS events in the TOS subsample (see fig. 10):

$$\epsilon_{TIS|TOS} = \frac{N_{TISTOS}}{N_{TOS}}. \tag{15}$$

Now, the most imporant step of the TISTOS-method must be made. At this point we make the following assumption: The occurrence of an event being labeled TIS, is completely random, i.e. a TIS event is a sign of the trigger inefficiency and the chance of its occurrence is therefore the same for every specified decay channel.

Then, the TIS efficiency of any subsample of triggered events is equal and

$$\epsilon_{TIS} \equiv \epsilon_{TIS|TOS}. \tag{16}$$

Now, we can rewrite eq. (15) to obtain;

$$\epsilon_{trig} = \frac{N_{trig}}{N_{TIS}} \cdot \epsilon_{TIS} = \frac{N_{trig}}{N_{TIS}} \cdot \frac{N_{TISTOS}}{N_{TOS}}, \tag{17}$$

where all quantities can be determined from the data.

Because of the limited time scope for this thesis, the calculation of the trigger efficiencies of L0 and HLT1, using the TISTOS method, could not be completed. Instead, the efficiency of HLT2, which requires less details of the rest of the analysis, was determined. This is discussed in the next section.

5.3 Performance of the HLT2 in the search for $B_0^{(s)} \to e^{\pm}\mu^{\mp}$

In the previous section we have seen how to determine the trigger efficiency using data only. In this section, the other method is shown, by means of simulation. The HLT2 efficiency is determined this way. This is possible because the online reconstruction of HLT2 in the trigger system and the offline reconstruction are almost identical. So it is known how the HLT2 selects events and can therefore be reproduced in a simulation.

From section 5.2 we know that the trigger efficiency can be defined as

$$\epsilon_{sel \to trig} = \frac{N_{sel \to trig}}{N_{sel}}. \tag{18}$$

In a simulation, the number of events in your final selection, N_{sel}, is known. A straightforward calculation can therefore be made to determine the efficiency. However, because the trigger system has three different levels, events still have to pass the L0 and HLT1 triggers before being analyzed by the HLT2. Therefore, L0 and HLT1 can be seen as the first step of the trigger process, HLT2 as the second step. So we rewrite eq. (19) to obtain:

$$\epsilon_{sel \to trig} = \epsilon_{sel \to \text{step 1}} \cdot \epsilon_{\text{step 1} \to \text{step 2}}. \tag{19}$$

In words this means that the efficiency of the total trigger system is equal to the efficiency of the first step, which is the number of events that passed L0 and HLT1 divided by the number of events that should have passed L0 and HLT1, multiplied by the efficiency of the second step, which is the number

of events, given that they have passed L0 and HLT1, now also pass HLT2, divided by the number of events that should have passed the HLT2.

So the following definition can be made:

$$\epsilon_{\text{HLT2}} \equiv \epsilon_{\text{step 1}\to\text{step 2}}. \tag{20}$$

To determine the HLT2 efficiency, the program ROOT was used. ROOT is a data analysis software framework developed at CERN.

The data from the simulation was stored in the form of a .root file. This .root file has the following structure. It contains tuples of data, with information about different important signal decays. In this case we are interested in the tuple `B2emuTuple`, as this contains all the information about $B_s^0 \to e^{\pm}\mu^{\mp}$.

Tuples can be further divided into leafs. Every leaf contains information about a specific quantity of the signal decay. For example, histograms of the momenta p, or transverse momenta p_T, of the electron, muon or B_s^0-meson. There are also leafs included with a yes or no decision, for TIS and TOS conditions on all the trigger lines. For example, in the L0 trigger, an event can be triggered on the muon requirements with trigger line name: `B_s0_L0MuonDecision`. Based on this, events can be categorized TOS or not (see fig. 11).

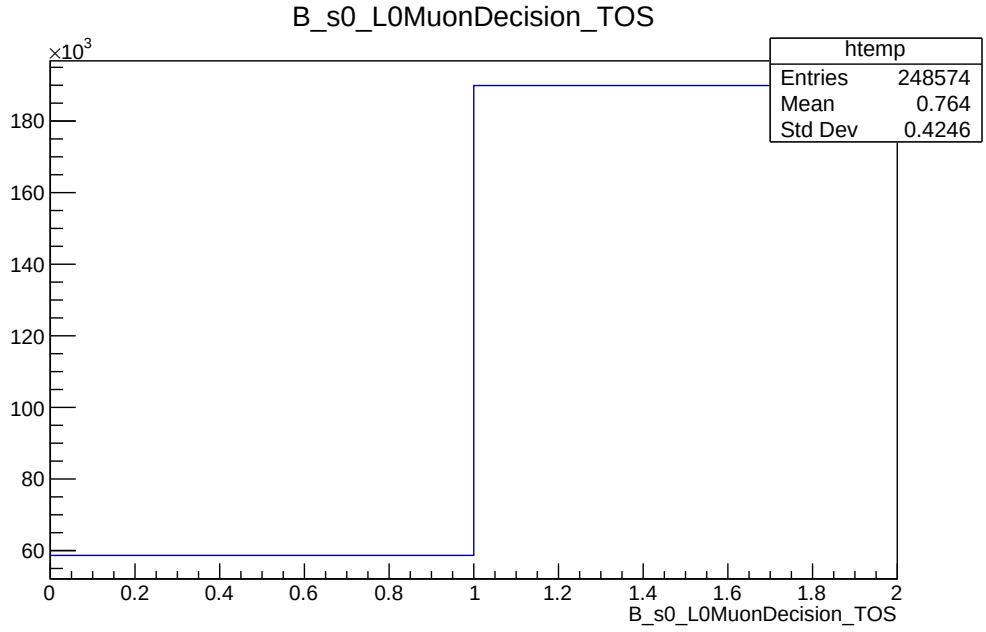

Figure 11: If events are categorized as TOS, they have a value of > 1. The events < 1 are not TOS, so they are TIS or TISTOS

Because the events triggered by the HLT2, first have to pass L0 and HLT1, the HTL2 decisions are conditional on the previous step. The method chosen to determine the efficiency of HLT2 is the same as the 2013 analysis [25]. The events are required to be TOS on the trigger line `L0MuonDecision` in L0, and TOS on either `Hlt1TrackMuon` or `Hlt1TrackAllMuonL0` in HLT1. The efficiencies of these lines were calculated in ROOT using Monte Carlo (MC) data and are listed in table 2.

The MC data is generated by first simulating a *pp* collision producing events. Then by simulating the interactions of particles with the detector. Finally by simulating how the trigger responds to these interactions. Data coming from the detector after this point is reconstructed and analyzed in the same way as real data, with the difference that it is known what the output should be. See [21] for more details on MC simulation. In this case, the MC data *only* consists of events including $B_s^0 \to e^{\pm}\mu^{\mp}$.

Trigger Line	TOS (%)
`L0MuonDecision`	76.4
`Hlt1TrackMuon`	84.9
`Hlt1TrackAllL0`	79.7
`TrackMuon || TrackAllL0`	91.0
`Hlt2TopoMu2Body`	82.4
`Hlt2Topo2Body`	76.7
`Hlt2B2HH`	49.3
`TopoMu2Body || Topo2Body || B2HH`	83.9

Because in the search for $B_s^0 \to e^{\pm}\mu^{\mp}$, topological trigger lines are considered important, the condition `TopoMu2Body || Topo2Body || B2HH`, given that the events also passed the L0 and HLT1 requirements, is defined as the efficiency of HLT2 [25]. Therefore, $\epsilon_{HLT2} = 83.9\%$.

In the previous section, the TISTOS method to obtain the L0+HLT1 efficiency was described. In this section, the way to obtain the HLT2 efficiency was given. To determine the total trigger efficiency of the LHCb detector in the search for $B_s^0 \to e^{\pm}\mu^{\mp}$, both are required. However, obtaining the L0+HLT1 efficiency requires detailed information of the complete analysis and could not be completed in the limited scope of this thesis.

6 Conclusion and Outlook

The goal of this research was to find out how the the trigger efficienies at LHCb can be determined. It was found that there are two methods to do this. A data-based method, called TISTOS method is preferred for the determination of the L0 and HLT1 efficiencies. Straightforward determination from simulation is preferred for the HLT2 efficiency. This is due to the fact that L0 and HLT1 do not use the complete offline reconstruction used in HLT2 and are therefore not well reproduced in a simulation.

It was shown how the TISTOS method works, as an alternative to simulation. The events that are stored are categorized in TIS, TOS and simultaneously TIS and TOS. With these categories, the determination of the efficiency can be rewritten in such a way, that all quantities can be obtained from data and no simulation is needed.

The determination of the HLT2 efficiency in the search for $B_s^0 \to e^{\pm}\mu^{\mp}$ was also given, using simulation. It was shown how this can be done by demanding TOS conditions on L0 and HLT1 trigger lines, as events first have to pass these trigger before they can be analyzed by the HLT2. The efficiency was determined to be $\epsilon_{HLT2} = 83.9\%$.

The L0+HLT1 efficiency could not be determined within the limited scope of this research project and will have to be determined later. Once both the L0+HLT1 and HLT2 efficiencies are known, the total trigger efficiency of the LHCb detector in the search for $B_s^0 \to e^{\pm}\mu^{\mp}$ can be determined. This is essential in determining the branching fraction of this decay channel. With the determination of this branching fraction, or by setting an upper limit on its maximal magnitude, insights on new physics models can possibly be gained.

References

[1] J. C. Morrison, *Modern Physics for Scientists and Engineers*. Academic Press, 2010.

[2] B. R. Martin, *Nuclear and Particle Physics*. Wiley, 2009.

[3] N. Cabibbo, "Unitary Symmetry and Leptonic Decays," *Phys. Rev. Lett.*, vol. 10, pp. 531–533, Jun 1963.

[4] M. Kobayashi and T. Maskawa, "CP-Violation in the Renormalizable Theory of Weak Interaction," *Prog. Theor. Phys.*, vol. 49, pp. 652–657, Feb 1973.

[5] A. Aguilar, L. B. Auerbach, R. L. Burman, *et al.*, "Evidence for Neutrino Oscillations from the Observation of Electron Anti-Neutrinos in a Muon Anti-Neutrino Beam," *Phys.Rev.D*, vol. 64:112007, 2001.

[6] Z. Maki, M. Nakagawa, and S. Sakata, "Remarks on the Unified Model of Elementary Particles," *Prog. Theor. Phys.*, vol. 28, pp. 870–880, Nov 1962.

[7] Y. Kuno and Y. Okada, "Muon Decay and Physics Beyond the Standard Model," *Rev.Mod.Phys.*, vol. 73:151-202, 2001.

[8] C. Vos, "Overview of the theoretical status of cLFV." http://irs.ub.rug.nl/dbi/55a36eb6daf4d, 2015.

[9] G. Arnison, A. Astbury, B. Aubert, *et al.*, "Experimental observation of isolated large transverse energy electrons with associated missing energy at $s = 540$ GeV," *Physics Letters B*, vol. 122, pp. 103–116, Feb 1983.

[10] P. W. Higgs, "Broken Symmetries and the Masses of Gauge Bosons," *Phys. Rev. Lett.*, vol. 13, pp. 508–509, Oct 1964.

[11] K. A. Ulmer, "Supersymmetry: Experimental Status," 2016.

[12] C. Langenbruch, "Rare decays at LHCb," 2016.

[13] CMS and LHCb Collaborations, "Observation of the rare $B_s^0 \to \mu^+\mu^-$ decay from the combined analysis of CMS and LHCb data," *Nature*, vol. 522,, pp. 68–72, 2014.

[14] R. Aaij, B. Adeva, M. Adinolfi, *et al.*, "Search for the lepton-flavour violating decays $B_s^0 \to e^\pm\mu^\mp$ and $B^0 \to e^\pm\mu^\mp$," *Phys.Rev.Lett.*, vol. 111 141801, 2013.

[15] B. Gripaios, M. Nardecchia, and S. Renner, "Linear flavour violation and anomalies in B physics," *Journal of High Energy Physics*, vol. 2016, Jun 2016.

[16] R. Aaij, B. Adeva, M. Adinolfi, *et al.*, "Search for the lepton-flavour violating decay $D_0 \to e^{\pm}\mu^{\mp}$," *Physics Letters B*, vol. 754, pp. 167–175, Mar 2016.

[17] M. Petrič, M. Starič, I. Adachi, *et al.*, "Search for leptonic decays of D^0-mesons," *Physical Review D*, vol. 81, May 2010.

[18] A. A. Alves, L. M. Andrade Filho, A. F. Barbosa, *et al.*, "The LHCb Detector at the LHC," *J. Inst.*, vol. 3, pp. S08005–S08005, Aug 2008.

[19] S. Tolk, *Discovery Of Rare B Decays: First observation of the $B_s^0 \to \mu^+\mu^-$ decay, first evidence of the $B^0 \to \mu^+\mu^-$ decay.* PhD thesis, 2016.

[20] A. Achilli, *et al.*, "Total and inelastic cross-sections at LHC at CM energy of 7 TeV and beyond," 2011.

[21] J. A. N. van Tilburg, *Track Simulation and Reconstruction in LHCb.* PhD thesis, Vrije U., Amsterdam, 2005.

[22] R. Aaij, J. Albrecht, F. Alessio, *et al.*, "The LHCb Trigger and its Performance in 2011," 2012.

[23] J. Albrecht, V. V. Gligorov, G. Raven, and S. Tolk, "Performance of the LHCb High Level Trigger in 2012," *J. Phys.: Conf. Ser.*, vol. 513, p. 012001, 2013.

[24] O. Callot and S. Hansmann-Menzemer, "The Forward Tracking: Algorithm and Performance Studies," Tech. Rep. LHCb-2007-015, May 2007.

[25] F. Archilli, G. Lanfranchi, and F. Soomro, "Search for the lepton-flavour violating decays $B_s^0 \to e^+\mu^-$ and $B^0 \to e^+\mu^-$," *LHCb-ANA-2012-079-v5*, 2013.